

Wave diffraction by a circular crack in an ice sheet floating on water of finite depth

Z. F. Li, G. X. Wu, and Y. Y. Shi

Citation: *Physics of Fluids* **30**, 117103 (2018); doi: 10.1063/1.5053563

View online: <https://doi.org/10.1063/1.5053563>

View Table of Contents: <http://aip.scitation.org/toc/phf/30/11>

Published by the *American Institute of Physics*

Articles you may be interested in

[Free vibration predicted using forced oscillation in the lock-in region](#)

Physics of Fluids **30**, 113601 (2018); 10.1063/1.5056203

[Numerical investigation of internal solitary waves of elevation type propagating on a uniform slope](#)

Physics of Fluids **30**, 116602 (2018); 10.1063/1.5050568

[Unsteady shock interactions on V-shaped blunt leading edges](#)

Physics of Fluids **30**, 116104 (2018); 10.1063/1.5051012

[Convergence of strong shock waves in non-ideal magnetogasdynamics](#)

Physics of Fluids **30**, 116105 (2018); 10.1063/1.5051589

[Letter: Galilean invariance of Rortex](#)

Physics of Fluids **30**, 111701 (2018); 10.1063/1.5058939

[Oscillation characteristics of mutually impinging dual jets in a mixing chamber](#)

Physics of Fluids **30**, 117102 (2018); 10.1063/1.5051731

PHYSICS TODAY

WHITEPAPERS

ADVANCED LIGHT CURE ADHESIVES

Take a closer look at what these environmentally friendly adhesive systems can do

READ NOW

PRESENTED BY
 MASTERBOND
ADHESIVES | SEALANTS | COATINGS

Wave diffraction by a circular crack in an ice sheet floating on water of finite depth

Z. F. Li,¹ G. X. Wu,^{1,2,a)} and Y. Y. Shi³

¹*School of Naval Architecture and Ocean Engineering, Jiangsu University of Science and Technology, Zhenjiang 212003, China*

²*Department of Mechanical Engineering, University College London, Torrington Place, London WC1E 7JE, United Kingdom*

³*College of Shipbuilding Engineering, Harbin Engineering University, Harbin 150001, China*

(Received 23 August 2018; accepted 31 October 2018; published online 20 November 2018)

The problem of wave diffraction by a circular crack in an ice sheet floating on water of finite depth is considered. The fluid flow is described by the linear velocity potential theory, while the infinitely extended ice sheet is modeled as a thin elastic plate with uniform properties. At the crack, zero bending moment and shear force conditions are enforced. The solution starts from the Green function for ice sheet without the crack. This is then used to obtain an integral equation, in which the jumps of the displacement and slope across the crack are the unknowns. For a circular crack, the unknowns are expanded into the Fourier series in the circumferential direction. Through imposing the boundary conditions at the crack, a matrix equation is obtained for the unknowns, which is then truncated and solved. Convergence study is undertaken with respect to the truncation, and it has been found that the series converges fast. A far field identity is used to verify the solution procedure and is found to be satisfied very accurately. Extensive results are provided, and their physical implications are discussed. These include the jumps of the displacement and slope across the crack, resonant motion, far field diffracted wave amplitude, and the deflection of the ice sheet. *Published by AIP Publishing.*
<https://doi.org/10.1063/1.5053563>

I. INTRODUCTION

The propagation of ocean waves through floating ice sheet has received considerable attentions increasingly, especially in the geophysical problems. This is due to the fact that the waves could have a significant impact on the seasonal changes in the morphology of the ice cover in polar regions.¹ In particular, the waves may fracture the large ice sheet into smaller ones through imposing sufficient flexural load, which may lead to an acceleration of the melt of sea ice. The physical process usually involves the wave/ice interactions, which is in many cases highly complex.² This is further complicated by the fact that the ice sheets in nature generally involve some imperfections, which may have an important effect on the wave propagations.

The field observations of Robin³ indicated that the large ice sheet could bend to let the wave pass through in a flexural-gravity waveform. The recent field measurements of Kohout *et al.*⁴ also showed that ocean waves could penetrate hundreds of kilometers into the ice-covered ocean. During the wave ice interactions, when the horizontal dimension of the ice sheet is much larger than the vertical one, it could be usually modeled as an elastic plate floating on the water surface. This has been demonstrated in the field experiments of Squire *et al.*⁵ Based on the elastic plate model for ice, Fox and Squire⁶ solved the oblique incident wave interaction with the homogeneous semi-infinite ice sheet. The water is of finite depth, and

the method adopted is the matched eigenfunction expansions (MEEs). A similar problem was also investigated by Balmforth and Craster⁷ through the Wiener-Hopf technique and by Linton and Chung⁸ through the residue calculus method. It was found that the wave transmission was the main result at the long wave period, while the wave reflection became negligible. Also, a critical incident angle existed, beyond which there would be no wave transmission into the ice sheet. When there was a fixed vertical wall at the end of semi-infinite ice sheet, Brocklehurst, Korobkin, and Părău⁹ constructed an analytical solution through the integral transform approach. The effects of some physical parameters, such as ice thickness and flexural-gravity wavelength, on the ice deflection and forces acting on the wall were investigated. Korobkin, Khabakhpasheva, and Papin¹⁰ also solved the problem that the longitudinally infinitely extended ice sheet was confined between two transverse parallel vertical walls. This could be used as a model for a river covered by an ice sheet, and the distributions of the strains as well as the wave profiles across the channel were investigated.

For an ice sheet of finite extent, Meylan and Squire¹¹ obtained the solution for a circular ice floe in an incident wave of infinite water depth, through the boundary integral equations. The features of ice deflections and scattering wave patterns surrounding the floe were investigated. The problem was then extended to the finite water depth by Pete, Meylan, and Chung.¹² Montiel *et al.*¹³ conducted a series of wave basin experiments for the flexural response of thin floating elastic discs of various thicknesses. The effects of the steepnesses and frequencies of the incident waves were studied. Some

^{a)} Author to whom correspondence should be addressed: g.wu@ucl.ac.uk. Tel.: +44 20 7679 3870. Fax: +44 20 7388 0180.

possible reasons for the discrepancy between the results from the numerical model and the experiment were further analyzed by Montiel *et al.*¹⁴ In the marginal ice zone, due to wave scattering and directional spreading, the wave energy may attenuate with respect to the propagation distance. To model this feature, Montiel, Squire, and Bennetts¹⁵ developed a solution for the wave scattering by tens of thousands of compliant circular ice floes based on that for a single one. The slab-clustering method was used, which was originally for wave interaction with multiple structures in open water. A flexural failure model was further introduced by Montiel and Squire¹⁶ to study the mechanisms of ice break up in the marginal ice zone. Through combining the boundary integral equation method for the fluid with the finite element method for the ice sheet, Wang and Meylan¹⁷ solved the interaction problem of an incident wave with an arbitrarily shaped ice floe.

A closely related problem is the wave scattering by a polynya, i.e., a finite open water region confined or surrounded by ice sheets. For the two dimensional (2D) problem, Williams and Squire¹⁸ considered the wave propagation through an ice sheet with three parts of different thicknesses. Both the Wiener-Hopf technique and residue calculus method were adopted to solve the problem. When the thickness of the middle sheet is taken to be zero, the solution is for a polynya. On the other hand, when the thicknesses of the two sheets on the two sides are taken to be zero, the solution is for an ice floe. In general, when the thicknesses of the three parts of the sheet are nonzero, the solution can be used for the case of a sudden change in ice thickness, for example an embedded iceberg. To investigate the effects of continuously varying ice thickness and depth on the wave propagation, Porter and Porter¹⁹ derived a procedure based on the variational principle for the governing equations of the problem. The solution was obtained by the Rayleigh-Ritz method. The derivation was carried out for the three dimensional (3D) problem, while results were given only for the 2D scattering problem for simplicity. By adopting the procedure in Porter and Porter,¹⁹ Bennetts, Biggs, and Porter²⁰ considered a similar problem and the solution procedure was improved by using a multi-mode expansion to approximate the velocity potential. The results provided were for obliquely incident wave upon 2D ice covers of both the infinite and finite extent. For the 3D problem, Bennetts and Williams²¹ solved the wave interactions with a polynya or an ice floe of an arbitrarily smooth shape, and the effects of the boundary geometry were investigated. In that solution procedure, the velocity potential was first expanded into a finite set of chosen modes in the vertical direction, and then the remained function in the 2D horizontal plane was solved via the variational principle.

In many cases, the ice sheet may also involve some imperfections and the crack is one of the examples. Through applying the MEE procedure similar to that in Fox and Squire,⁶ Barrett and Squire²² solved the problem of oblique incident wave interaction with a crack in the 2D ice sheet of finite water depth. They found that when the properties of the ice sheet on both sides of the crack were the same, there would be a period at which perfect transmission would occur. It may be noticed that for oblique incident wave interaction with a straight crack of

infinite extent on both sides, the three dimensional governing Laplace equation for the velocity potential can be transformed into the two dimensional Helmholtz equation. By using the Green function for the 2D ice sheet without the crack, Squire and Dixon²³ developed an analytical model for the normal incident wave of infinite water depth, and explicit formulas for the reflection and transmissions coefficients were obtained. The procedure was further extended by Williams and Squire²⁴ for the oblique incident wave. By first separating the problem into the sum of symmetric and antisymmetric parts, Evans and Porter²⁵ developed the series form solution for the problem similar to that in the work of Barrett and Squire.²² The edge waves traveling along the crack were found to be possible. By introducing a pair of source functions for a single crack, Porter and Evans²⁶ derived the solution for a finite crack with an arbitrary shape in the ice sheet for the 3D problem. However, as stated by the authors of that paper, due to the complexity of the kernels of the integrand involved in the solution procedure, only the results for a finite straight line crack were provided. The problem was further extended to the wave interactions with multiple parallel straight line cracks of infinite length²⁷ for the 2D case and finite length²⁸ for the 3D case. Li, Wu, and Ji²⁹ derived the Green function for a 2D ice sheet with the crack in an integral form, which satisfied edge conditions at the crack. This allowed the solutions due to multipoles to be obtained directly by taking the derivatives with respect to the source position, which were used to construct the solution for a submerged circular cylinder.²⁹ The Green function was further extended and used in the boundary element method for a body of an arbitrary shape submerged below an ice sheet with multiple cracks.³⁰

In all of the above studies, the crack is assumed to be 2D or straight lines in 3D, and very little work seems to have been done for the 3D problem of an ice sheet with a curved crack. In this work, we shall consider the case of wave interaction with a crack of curvature. The principle of the developed method can be applied to a crack line of an arbitrary shape. Here, we shall focus on the crack with a circular shape. This allows the solution to be obtained analytically in an explicit form involving some integrations of Bessel functions. From the solution, the nature of the wave diffraction by a closed crack can be established. In particular, through the analytical expression, the oscillatory behaviors and the peaks of ice deflection can be related to the modes of the deflection.

The rest of the paper is arranged as follows. The linearized velocity potential problem for the wave interaction with a curvilinear crack is presented in Sec. II, and zero bending moment and shear force conditions at the crack are described. The Green function for an infinite ice sheet with finite water depth is first presented in Sec. III A. Then through applying Green's identity, the diffracted velocity potential is written in an integral form with two sets of unknown coefficients in Sec. III B, which can be further determined through applying the crack conditions. The far field diffracted wave amplitude and the so-called scattering cross section equation are derived in Sec. III C. In Sec. IV, various numerical results are presented and discussed. Conclusions are drawn in Sec. V.

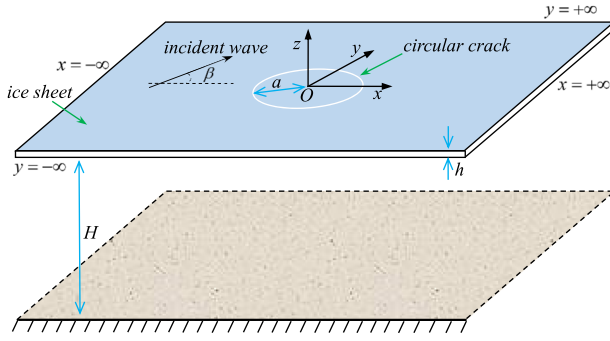


FIG. 1. Coordinate system and sketch of the problem.

II. MATHEMATICAL MODEL

We consider the problem of wave interaction with an ice sheet of infinite extent, with a circular crack of radius a , as sketched in Fig. 1. A Cartesian coordinate system $O-xyz$ is defined, with the origin O at the centre of the circular ice sheet inside the crack, x -axis along the undisturbed mean flat interface surface of water and ice sheet, and z -axis pointing vertically upwards. The propagation direction of the flexural-gravity incident wave from infinity is assumed to from an angle β with the x -axis, as shown in Fig. 1, and the water depth H is assumed to be constant.

The fluid is assumed to be inviscid, incompressible, and homogeneous, and its motion is assumed to be irrotational. Thus the velocity potential Φ can be introduced to describe the fluid flow. When the amplitude of wave motion is small compared to its length, the linearized velocity potential theory can be further used. Under the assumption that the motion is sinusoidal in time with radian frequency ω , the total velocity potential can be written as³¹

$$\Phi(x, y, z, t) = \text{Re}(\phi e^{i\omega t}), \quad (1)$$

where $\phi = \phi_I + \phi_D$ with ϕ_I as the incident potential and ϕ_D as the diffracted potential by the circular crack. Mass conservation requires that the potential ϕ satisfies the Laplace equation throughout the fluid or

$$\nabla^2 \phi = \nabla_H^2 \phi + \frac{\partial^2 \phi}{\partial z^2} = 0, \quad (2)$$

where ∇_H^2 is the Laplacian in the horizontal plane

$$\nabla_H^2 = \frac{\partial^2}{\partial x^2} + \frac{\partial^2}{\partial y^2}. \quad (3)$$

The ice sheet is modeled as a continuous thin elastic plate with uniform properties, i.e., Young's modulus E , Poisson's ratio ν , density ρ_i , and thickness h are all constant. The rational and justification as well as the limitation for the fluid flow model and the ice sheet model have been extensively discussed in the previous work, for example by Squire *et al.*³² and Squire.^{2,33} Assuming that there is no air gap between the ice sheet and the ocean surface, through combing the kinematic condition of the same vertical velocity with the dynamic condition of ice sheet deformation due to fluid pressure, the boundary condition on their interface can be given as²

$$(L\nabla_H^4 + \rho_w g - m\omega^2) \frac{\partial \phi}{\partial z} - \rho_w \omega^2 \phi = 0 \quad (r \neq a, z = 0), \quad (4)$$

where $r^2 = x^2 + y^2$, $L = Eh^3/[12(1 - \nu^2)]$ and $m = \rho_i h$ are the effective flexural rigidity and mass per unit area of the ice sheet, respectively, ρ_w is the density of water, and g is the acceleration due to gravity. At the ice crack, we assume that the edges of the ice sheet are free to move, which provides the following two conditions based on zero bending moment and zero shear force

$$B\left(\frac{\partial \phi}{\partial z}\right) = 0 \quad \text{and} \quad S\left(\frac{\partial \phi}{\partial z}\right) = 0 \quad (r = a, z = 0), \quad (5)$$

where

$$B = \nabla_H^2 - \nu_0(\sin^2 \theta \frac{\partial^2}{\partial x^2} + \cos^2 \theta \frac{\partial^2}{\partial y^2} - \sin 2\theta \frac{\partial^2}{\partial x \partial y}), \quad (6)$$

$$S = \frac{\partial}{\partial n} \nabla_H^2 + \nu_0 \frac{\partial}{\partial s} [\cos 2\theta \frac{\partial^2}{\partial x \partial y} + \frac{\sin 2\theta}{2} (\frac{\partial^2}{\partial y^2} - \frac{\partial^2}{\partial x^2})], \quad (7)$$

$\nu_0 = 1 - \nu$, and θ is the angle between the positive x axis and the normal vector $\vec{n} = (n_x, n_y)$ of the crack, pointing outwards. Here, the edge condition is on the basis that the inner ice sheet is completely detached form the outer ice sheet. For other physical broken conditions, different mathematical conditions may have to be used. On the seabed, the following impermeable condition should be enforced:

$$\frac{\partial \phi}{\partial z} = 0 \quad (z = -H). \quad (8)$$

The radiation condition at infinity requires the wave to propagate outwards or

$$\lim_{r \rightarrow \infty} \sqrt{r} \left(\frac{\partial \phi_D}{\partial r} + ik_0 \phi_D \right) = 0, \quad (9)$$

where k_0 is the positive real root of the dispersion equation $K(\omega, k_0) = 0$ for the flexural gravity wave in the ice sheet, and

$$K(\omega, k) \equiv (Lk^4 + \rho_w g - m\omega^2)k \tanh(kH) - \rho_w \omega^2. \quad (10)$$

It may be noticed that apart from a pair of real roots $\pm k_0$, there are a sequence of purely imaginary roots $\pm k_n$ with $n = 1, 2, \dots$ and four complex roots $\pm k_{-1}$ and $\pm k_{-2}$ symmetric about the real and imaginary axes.

Finally, we should note that the adopted mathematical model is consistent with those adopted by others.² The rational and justification of the model has been discussed through the results from field experiment and field observation.⁵

III. SOLUTION PROCEDURES

A. The Green function for an ice sheet without the crack

By following the procedure in the work of Wehausen and Laitone³⁴ for the free surface problem, we may seek the solution of the Green function G in the following form:

$$G = G_0 + G_1, \quad (11)$$

where

$$G_0 = \frac{1}{r_1} + \frac{1}{r_2} \quad (12)$$

is the potential at point $p(x, y, z)$ due to a sink at point $q(\xi, \eta, \zeta)$ and its mirror image q' about the flat seabed $z = -H$. Here r_1 is the distance between p and q , while r_2 is the distance between p and q' . G_0 satisfies the condition on the flat seabed, and G_1

is introduced to satisfy the condition on the ice sheet and the radiation condition at infinity. In order to derive G_1 , we may write G_0 as³⁴

$$G_0 = \int_0^{+\infty} [e^{-k|z-\xi|} + e^{-k(z+\xi+2H)}] J_0(kR) dk, \quad (13)$$

where $R^2 = (x - \xi)^2 + (y - \eta)^2$ and $J_0(kR)$ is the Bessel function.³⁵ To satisfy the condition on the ice sheet, we may write G_1 as

$$G_1 = \int_0^{+\infty} A(k) Z(z) J_0(kR) dk, \quad (14)$$

where

$$Z(z) = \cosh[k(z + H)]. \quad (15)$$

Substituting Eqs. (13) and (14) into Eq. (4) and using $\nabla_H^4 \phi = -\partial^2(\nabla_H^2 \phi)/\partial z^2 = \partial^4 \phi/\partial z^4$, we can obtain

$$A(k) = \frac{2P(k)e^{-kH}}{K(\omega, k)Z(0)} Z(\xi), \quad (16)$$

where

$$P(k) = (Lk^4 + \rho_w g - m\omega^2)k + \rho_w \omega^2. \quad (17)$$

Substituting Eq. (16) into Eq. (14), and then the result together with Eq. (12) into Eq. (11), we have

$$G = \frac{1}{r_1} + \frac{1}{r_2} + \int_L \frac{2P(k)e^{-kH}}{K(\omega, k)Z(0)} Z(\xi) Z(z) J_0(kR) dk, \quad (18)$$

where L is the integral route from 0 to $+\infty$ and it passes over the pole at $k = k_0$, at which $K(\omega, k_0) = 0$, to satisfy the radiation condition in Eq. (9). By following the procedure in Appendix A of Li, Wu, and Ji,³⁰ it can be shown that in a reversed way when (x, y, z) is fixed, G also satisfies the boundary conditions for varying (ξ, η, ζ) .

B. Wave scattering by a circular crack

For the circular crack, we introduce the following polar coordinate system:

$$x = r \cos \theta \text{ and } y = r \sin \theta, \quad \xi = r_0 \cos \theta_0 \text{ and } \eta = r_0 \sin \theta_0. \quad (19)$$

In such a case, the direction of n in Eqs. (6) and (7) is the same as that of r , and these two equations can be written as

$$B = \nabla_H^2 - \nu_0 \left(\frac{1}{r} \frac{\partial}{\partial r} + \frac{1}{r^2} \frac{\partial^2}{\partial \theta^2} \right), \quad (20)$$

$$S = \frac{\partial}{\partial r} \nabla_H^2 + \frac{\nu_0}{r} \left(\frac{1}{r} \frac{\partial^3}{\partial \theta^2 \partial r} - \frac{1}{r^2} \frac{\partial^2}{\partial \theta^2} \right), \quad (21)$$

with

$$\nabla_H^2 = \frac{\partial^2}{\partial r^2} + \frac{1}{r} \frac{\partial}{\partial r} + \frac{1}{r^2} \frac{\partial^2}{\partial \theta^2}. \quad (22)$$

Applying the Green's identity to G and ϕ_D , we have

$$4\pi \phi_D(\xi, \eta, \zeta) = \int_S [G(x, y, z; \xi, \eta, \zeta) \frac{\partial \phi_D(x, y, z)}{\partial n} - \phi_D(x, y, z) \frac{\partial G(x, y, z; \xi, \eta, \zeta)}{\partial n}] ds, \quad (23)$$

where the fluid boundary S is comprised of the sea bed S_b , the entire ice sheet S_i , and a vertical cylindrical surface at infinity S_∞ . It may be noticed on the right-hand side of Eq. (23) that both the normal derivative in the integrand and the integration

are carried out with respect to the field point (x, y, z) . Noticing that both G and $\phi_D(x, y, z)$ satisfy the conditions in Eqs. (8) and (9) on S_b and S_∞ , respectively, we have that only the integral over the ice sheet S_i is nonzero in Eq. (23), and thus

$$4\pi \phi_D = \int_{S_i} \left(G \frac{\partial \phi_D}{\partial z} - \phi_D \frac{\partial G}{\partial z} \right) ds. \quad (24)$$

Invoking the condition in Eq. (4), we have

$$\varphi = \frac{L}{\rho_w \omega^2} \nabla_H^4 \frac{\partial \varphi}{\partial z} + \frac{\rho_w g - m\omega^2}{\rho_w \omega^2} \frac{\partial \varphi}{\partial z} \quad \text{on } S_i, \quad (25)$$

where φ can be either G or $\phi_D(x, y, z)$. Substituting Eq. (25) into Eq. (24), we obtain

$$4\pi \phi_D = \frac{L}{\rho_w \omega^2} \int_{S_i} \left(\frac{\partial \phi_D}{\partial z} \nabla_H^4 \frac{\partial G}{\partial z} - \frac{\partial G}{\partial z} \nabla_H^4 \frac{\partial \phi_D}{\partial z} \right) ds. \quad (26)$$

Through applying Gauss's theorem, we have

$$\begin{aligned} \int_S f_b \nabla_H^4 f_a ds &= \int_S f_a \nabla_H^4 f_b ds + \int_C \left(f_b \frac{\partial \nabla_H^2 f_a}{\partial n} - \frac{\partial f_b}{\partial n} \nabla_H^2 f_a \right. \\ &\quad \left. + \frac{\partial f_a}{\partial n} \nabla_H^2 f_b - f_a \frac{\partial \nabla_H^2 f_b}{\partial n} \right) dl, \end{aligned} \quad (27)$$

where C is the closed boundary line of surface S in O - xy plane, and

$$f_a = \frac{\partial G}{\partial z} \text{ and } f_b = \frac{\partial \phi_D}{\partial z} \quad (z = 0). \quad (28)$$

Taking S as the ice sheet located inside and outside of the crack, respectively, and noticing that the line integral along the curve at infinity is zero, once the condition in Eq. (9) is adopted, we can write Eq. (26) as

$$\begin{aligned} 4\pi \phi_D &= \frac{L}{\rho_w \omega^2} \int_{C_i} \left(f_b \frac{\partial \nabla_H^2 f_a}{\partial n} - \frac{\partial f_b}{\partial n} \nabla_H^2 f_a \right. \\ &\quad \left. + \frac{\partial f_a}{\partial n} \nabla_H^2 f_b - f_a \frac{\partial \nabla_H^2 f_b}{\partial n} \right)_{-} dl, \end{aligned} \quad (29)$$

or

$$\begin{aligned} 4\pi \phi_D &= \frac{aL}{\rho_w \omega^2} \int_{-\pi}^{+\pi} \left(f_b \frac{\partial \nabla_H^2 f_a}{\partial r} - \frac{\partial f_b}{\partial r} \nabla_H^2 f_a \right. \\ &\quad \left. + \frac{\partial f_a}{\partial r} \nabla_H^2 f_b - f_a \frac{\partial \nabla_H^2 f_b}{\partial r} \right)_{r=a^-}^{r=a^+} d\theta, \end{aligned} \quad (30)$$

for a circular crack, where $-$ and $+$ indicate that the crack is approached from the inside and outside ice sheets, respectively. Here, it may be noticed that the relation $\partial/\partial n = \partial/\partial r$ at the circular crack has been used in Eq. (30). Substituting $\phi = \phi_I + \phi_D$ into Eq. (5), we have at $r = a$ and $z = 0$

$$\nabla_H^2 f_b = \nu_0 \left(\frac{1}{r} \frac{\partial}{\partial r} + \frac{1}{r^2} \frac{\partial^2}{\partial \theta^2} \right) f_b - B \left(\frac{\partial \phi_I}{\partial z} \right), \quad (31)$$

$$\frac{\partial}{\partial r} \nabla_H^2 f_b = -\frac{\nu_0}{r} \left(\frac{1}{r} \frac{\partial^3}{\partial \theta^2 \partial r} - \frac{1}{r^2} \frac{\partial^2}{\partial \theta^2} \right) f_b - S \left(\frac{\partial \phi_I}{\partial z} \right). \quad (32)$$

Substituting the above two equations into Eq. (30), and noticing that both G and ϕ_I are continuous across the crack, we have

$$4\pi \phi_D = \frac{aL}{\rho_w \omega^2} \int_{-\pi}^{+\pi} [D_d(f_b) - D_s \left(\frac{\partial f_b}{\partial r} \right)]_{r=a^-}^{r=a^+} d\theta, \quad (33)$$

where

$$D_d = \frac{\partial \nabla_H^2 f_a}{\partial r} + \frac{\nu_0}{r^2} \left(\frac{\partial f_a}{\partial r} - \frac{f_a}{r} \right) \frac{\partial^2}{\partial \theta^2}, \quad (34)$$

$$D_s = \nabla_H^2 f_a - \frac{\nu_0}{r} \frac{\partial f_a}{\partial r} - \frac{\nu_0 f_a}{r} \frac{\partial^2}{\partial \theta^2}. \quad (35)$$

At the circular crack, we can expect that both the displacement and the slope in the r direction are discontinuous. Their jumps may be expressed in the following Fourier series, respectively:

$$(f_b)_{r=a^+}^{r=a^-} = \sum_{\ell=-\infty}^{+\infty} A_\ell e^{i\ell\theta} \quad \text{and} \quad \left(\frac{\partial f_b}{\partial r} \right)_{r=a^+}^{r=a^-} = \sum_{\ell=-\infty}^{+\infty} B_\ell e^{i\ell\theta}. \quad (36)$$

Invoking Eq. (18) together with Eq. (13), we have

$$\frac{\partial G}{\partial z} = 2\rho_w \omega^2 \int_L \frac{\tanh(kH) + 1}{K(\omega, k)} k e^{-kH} Z(\zeta) J_0(kR) dk \quad (z = 0), \quad (37)$$

Applying Graf's theorem³⁵

$$J_0(kR) = \sum_{\ell=-\infty}^{+\infty} J_\ell(kr) J_\ell(kr_0) e^{-i\ell(\theta-\theta_0)}, \quad (38)$$

we can rewrite Eq. (37) as

$$\begin{aligned} \frac{\partial G}{\partial z} &= 2\rho_w \omega^2 \sum_{\ell=-\infty}^{+\infty} e^{-i\ell\theta} e^{i\ell\theta_0} \\ &\times \int_L \frac{\tanh(kH) + 1}{K(\omega, k)} k e^{-kH} Z(\zeta) J_\ell(kr) J_\ell(kr_0) dk \quad (z = 0). \end{aligned} \quad (39)$$

Substituting Eqs. (39) and (36) into Eq. (33), we can obtain

$$\begin{aligned} \phi_D &= \frac{L}{a^2} \sum_{\ell=-\infty}^{+\infty} e^{i\ell\theta_0} \int_L \frac{kZ(\zeta)}{K(\omega, k)Z(0)} J_\ell(kr_0) \\ &\times [A_\ell F_1(k, \ell) - B_\ell F_2(k, \ell)] dk, \end{aligned} \quad (40)$$

where

$$F_1(k, \ell) = -a^3 k^3 J_\ell^{(1)}(ka) - a\nu_0 \ell^2 k J_\ell^{(1)}(ka) + \nu_0 \ell^2 J_\ell(ka), \quad (41)$$

$$F_2(k, \ell) = -a^3 k^2 J_\ell(ka) - a^2 \nu_0 k J_\ell^{(1)}(ka) + a\nu_0 \ell^2 J_\ell(ka). \quad (42)$$

Here, the superscript (1) of J_ℓ means the first order derivative with respect to its argument. From Eq. (40), it can be seen that there are still two sets of unknown coefficients A_ℓ and B_ℓ , which can be determined through applying the conditions at the crack in Eqs. (31) and (32). To do this, we may use

$$e^{\pm ikr \cos \vartheta} = \sum_{\ell=-\infty}^{+\infty} (\pm i)^\ell J_\ell(kr) e^{i\ell\vartheta}, \quad (43)$$

to write the incident potential ϕ_I into the following form:

$$\begin{aligned} \phi_I &= I\psi(\zeta) e^{-ik_0 r_0 \cos(\theta_0 - \beta)} \\ &= I\psi(\zeta) \sum_{\ell=-\infty}^{+\infty} (-i)^\ell J_\ell(k_0 r_0) e^{i\ell\theta_0} e^{-i\ell\beta}, \end{aligned} \quad (44)$$

where

$$I = i\omega \frac{\Lambda}{k_0} \quad \text{and} \quad \psi(\zeta) = \frac{\cosh[k_0(\zeta + H)]}{\sinh(k_0 H)}. \quad (45)$$

Here, Λ is the amplitude of the incident wave. For a circular crack, the wave direction β becomes unnecessary as physics

of the problem will remain the same for any β . Thus without loss of generality, we take $\beta = 0$. This indicates

$$A_\ell = A_{-\ell} \quad \text{and} \quad B_\ell = B_{-\ell}. \quad (46)$$

Thus, in the following text, we need to consider the case for $\ell \geq 0$ only. Substituting Eqs. (40) and (44) into Eqs. (31) and (32), and using the orthogonality of $e^{-i\ell\theta_0}$, we have

$$A_\ell I_B^A(\ell) - B_\ell I_B^B(\ell) = I_B(\ell), \quad (47)$$

$$A_\ell I_S^A(\ell) - B_\ell I_S^B(\ell) = I_S(\ell), \quad (48)$$

where

$$I_B^A(\ell) = \frac{L}{a^2} \lim_{\substack{\zeta \rightarrow 0^- \\ r_0 \rightarrow a}} \int_L \frac{kZ^{(1)}(\zeta)}{K(\omega, k)Z(0)} F_B(k, \ell, r_0) F_1(k, \ell) dk, \quad (49)$$

$$I_B^B(\ell) = \frac{L}{a^2} \lim_{\substack{\zeta \rightarrow 0^- \\ r_0 \rightarrow a}} \int_L \frac{kZ^{(1)}(\zeta)}{K(\omega, k)Z(0)} F_B(k, \ell, r_0) F_2(k, \ell) dk, \quad (50)$$

$$I_B(\ell) = -I\psi^{(1)}(0)(-i)^\ell F_B(k_0, \ell, a), \quad (51)$$

and

$$I_S^A(\ell) = \frac{L}{a^2} \lim_{\substack{\zeta \rightarrow 0^- \\ r_0 \rightarrow a}} \int_L \frac{kZ^{(1)}(\zeta)}{K(\omega, k)Z(0)} F_S(k, \ell, r_0) F_1(k, \ell) dk, \quad (52)$$

$$I_S^B(\ell) = \frac{L}{a^2} \lim_{\substack{\zeta \rightarrow 0^- \\ r_0 \rightarrow a}} \int_L \frac{kZ^{(1)}(\zeta)}{K(\omega, k)Z(0)} F_S(k, \ell, r_0) F_2(k, \ell) dk, \quad (53)$$

$$I_S(\ell) = -I\psi^{(1)}(0)(-i)^\ell F_S(k_0, \ell, a), \quad (54)$$

with

$$F_B(k, \ell, r_0) = -k^2 J_\ell(kr_0) - \frac{\nu_0}{r_0} k J_\ell^{(1)}(kr_0) + \frac{\nu_0}{r_0^2} \ell^2 J_\ell(kr_0), \quad (55)$$

$$F_S(k, \ell, r_0) = -k^3 J_\ell^{(1)}(kr_0) - \frac{\nu_0}{r_0^2} \ell^2 k J_\ell^{(1)}(kr_0) + \frac{\nu_0}{r_0^3} \ell^2 J_\ell(kr_0). \quad (56)$$

We notice that if $\zeta = 0$ is taken directly in the integrands of Eqs. (49) and (50), the integrals become divergent. Thus we may take the limit of $\zeta \rightarrow 0$ in a manner similar to that in Li, Wu, and Ji,²⁹ and the details are given in Appendix A. Invoking Eq. (A15), we can rewrite Eqs. (49) and (50) as

$$\begin{aligned} I_B^A(\ell) &= \int_L \frac{1}{K(\omega, k)} \left\{ \frac{L}{a^4} \ell^2 \nu_0 (\ell^2 \nu_0 - a^2 k^2) K_1 [J_\ell(ka)]^2 \right. \\ &\quad + \nu_0 k \left(\frac{L}{a^2} \ell^2 \nu_0 k K_1 + K_2 \right) [J_\ell^{(1)}(ka)]^2 - \left[\frac{L}{a^3} \ell^2 (\ell^2 + 1) \right. \\ &\quad \left. \left. \times \nu_0^2 k K_1 - a k^2 K_2 \right] J_\ell^{(1)}(ka) J_\ell(ka) \right\} dk - \frac{\nu_0 \ell}{2a^2}, \end{aligned} \quad (57)$$

and

$$\begin{aligned} I_B^B(\ell) &= \int_L \frac{1}{K(\omega, k)} \left\{ \left[\frac{L}{a^3} \ell^2 \nu_0 (\ell^2 \nu_0 - 2a^2 k^2) K_1 + a k K_2 \right] \right. \\ &\quad \left. \times [J_\ell(ka)]^2 + \frac{L}{a} \nu_0^2 k^2 K_1 [J_\ell^{(1)}(ka)]^2 \right. \\ &\quad \left. - \nu_0 \left(\frac{L}{a^2} 2\ell^2 \nu_0 k K_1 - 2K_2 \right) J_\ell^{(1)}(ka) J_\ell(ka) \right\} dk - \frac{\nu_0}{a} \delta_{\ell 0}, \end{aligned} \quad (58)$$

where $\delta_{\ell 0}$ is the Kronecker delta function,

$$K_1 = k^2 \tanh(kH) \quad \text{and} \quad K_2 = \rho_w \omega^2 - (\rho_w g - m\omega^2) k \tanh(kH). \quad (59)$$

Similarly, we can rewrite Eqs. (52) and (53) as

$$I_S^A(\ell) = \int_L \frac{1}{K(\omega, k)} \left\{ \frac{L}{a^5} \ell^4 \nu_0^2 K_1 [J_\ell(ka)]^2 + \frac{1}{a} \left[\frac{L}{a^2} \ell^4 \nu_0^2 k^2 K_1 + (2\ell^2 \nu_0 + a^2 k^2) k K_2 \right] [J_\ell^{(1)}(ka)]^2 - \frac{2\ell^2 \nu_0}{a^2} \left(\frac{L}{a^2} \ell^2 \nu_0 k K_1 + K_2 \right) J_\ell^{(1)}(ka) J_\ell(ka) \right\} dk - \frac{\nu_0 \ell^3}{a^3}, \quad (60)$$

and

$$I_S^B(\ell) = \int_L \frac{1}{K(\omega, k)} \left\{ \frac{L}{a^4} \ell^2 \nu_0 (\nu_0 \ell^2 - a^2 k^2) K_1 [J_\ell(ka)]^2 + \nu_0 k \left[\frac{L}{a^2} \ell^2 \nu_0 k K_1 + K_2 \right] [J_\ell^{(1)}(ka)]^2 - k \left[\frac{L}{a^3} \ell^2 \nu_0^2 (\ell^2 + 1) \times K_1 - ak K_2 \right] J_\ell^{(1)}(ka) J_\ell(ka) \right\} dk - \frac{\nu_0 \ell}{2a^2}. \quad (61)$$

When the results of these integrals are obtained, the unknown coefficients A_ℓ and B_ℓ can be obtained from Eqs. (47) and (48). It may be noticed that from Eqs. (57)–(61), we have $I_B^A(\ell)$ and $I_B^B(\ell)$, $I_S^A(\ell)$ and $I_S^B(\ell)$ are of order ℓ^4 , while from Eqs. (51) and (54), we have $I_B(\ell)$ and $I_S(\ell)$ are of order ℓ^2 . Then invoking Eqs. (47) and (48), we have that both A_ℓ and B_ℓ decay in the order of $1/\ell^2$, which means that the two infinite series in Eq. (36) are convergent.

After ϕ_D is found, we can obtain the ice deflection through $W = \text{Re}[(\eta_I + \eta_D)e^{i\omega t}]$, where $\eta_I = Ae^{-ik_0 r_0 \cos(\theta_0)}$ is the incident wave, while η_D is due to the wave diffraction by the crack and can be obtained through the kinematic boundary condition on the ice sheet or

$$\eta_D = \frac{1}{i\omega} \left(\frac{\partial \phi_D}{\partial \zeta} \right)_{\zeta=0}. \quad (62)$$

Substituting Eq. (40) into the above equation, we have

$$\eta_D = \frac{1}{i\omega} \frac{L}{a^2} \sum_{\ell=-\infty}^{+\infty} e^{i\ell\theta_0} \int_L \frac{kZ^{(1)}(0)}{K(\omega, k)Z(0)} J_\ell(kr_0) \times [A_\ell F_1(k, \ell) - B_\ell F_2(k, \ell)] dk, \quad (63)$$

where the superscript (1) of Z means the first order derivative with respect to its argument, as used previously for J_ℓ .

C. Far field behavior of the diffracted wave

For the wave diffraction problem, a particular interest is the behaviors of the diffracted wave in the far field or $r_0 \rightarrow +\infty$, which allows us to catch some key properties of the scattering source. By applying³⁴

$$\text{P.V.} \int_0^{+\infty} f(k) \frac{e^{i[r_0(k-k_0)]}}{k-k_0} dk = i\pi f(k_0) \quad \text{for } r_0 \rightarrow +\infty \quad (64)$$

to Eq. (40), together with the asymptotic expansion of the Bessel function, we obtain

$$\lim_{r_0 \rightarrow +\infty} \phi_D = -i\pi k_0 \frac{L}{a^2} \sqrt{\frac{2}{\pi k_0 r_0}} \frac{e^{-i(k_0 r_0 - \pi/4)} \cosh[k_0(\zeta + H)]}{K'(\omega, k_0) \cosh(k_0 H)} \times \sum_{\ell=-\infty}^{+\infty} e^{i\ell(\theta_0 + \pi/2)} [A_\ell F_1(k_0, \ell) - B_\ell F_2(k_0, \ell)]. \quad (65)$$

Similar to Mei, Stiassnie, and Yue³¹ for the free surface problem, we may write the diffracted velocity potential ϕ_D in the far field as

$$\lim_{r_0 \rightarrow +\infty} \phi_D = \sqrt{\frac{2}{\pi k_0 r_0}} e^{-i(k_0 r_0 - \pi/4)} I U(\theta_0) \frac{\cosh[k_0(\zeta + H)]}{\sinh(k_0 H)}, \quad (66)$$

where

$$U(\theta_0) = -i\pi \frac{k_0 \tanh(k_0 H)}{I K'(\omega, k_0)} \frac{L}{a^2} \sum_{\ell=-\infty}^{+\infty} e^{i\ell(\theta_0 + \pi/2)} \times [A_\ell F_1(k_0, \ell) - B_\ell F_2(k_0, \ell)]. \quad (67)$$

Here, it may be noticed that $U(\theta_0)$ in the above equation reflects the scattered energy distribution along the circumferential direction. Thus, we may introduce

$$F = \frac{1}{2\pi} \int_{-\pi}^{+\pi} |U(\theta_0)|^2 d\theta_0, \quad (68)$$

which is a measure of the total scattered energy.

The far field behavior could also be used as a partial verification of the solution procedure and numerical results. Applying Green's theorem to the potential ϕ and its complex conjugation $\bar{\phi}$, we have

$$\int_S \left(\phi \frac{\partial \bar{\phi}}{\partial n} - \bar{\phi} \frac{\partial \phi}{\partial n} \right) ds = 0. \quad (69)$$

Similar to Eq. (29), invoking the boundary conditions on S_b , S_i , and S_∞ , then applying the Gauss theorem to the integral over S_i , we have

$$\frac{aL}{\rho_w \omega^2} \int_{-\pi}^{+\pi} \left[\frac{\partial \bar{\phi}}{\partial \zeta} \frac{\partial \nabla_H^2 (\frac{\partial \phi}{\partial \zeta})}{\partial r_0} - \frac{\partial^2 \bar{\phi}}{\partial r_0 \partial \zeta} \nabla_H^2 \left(\frac{\partial \phi}{\partial \zeta} \right) + \left(\frac{\partial^2 \phi}{\partial r_0 \partial \zeta} \right) \nabla_H^2 \frac{\partial \bar{\phi}}{\partial \zeta} - \frac{\partial \phi}{\partial \zeta} \frac{\partial \nabla_H^2 (\frac{\partial \bar{\phi}}{\partial \zeta})}{\partial r_0} \right]_{a^+} d\theta_0 + \frac{L}{\rho_w \omega^2} \times \int_{C_\infty} \left[\frac{\partial \bar{\phi}}{\partial \zeta} \frac{\partial \nabla_H^2 (\frac{\partial \phi}{\partial \zeta})}{\partial r_0} - \frac{\partial \phi}{\partial \zeta} \frac{\partial \nabla_H^2 (\frac{\partial \bar{\phi}}{\partial \zeta})}{\partial r_0} + \left(\frac{\partial^2 \phi}{\partial r_0 \partial \zeta} \right) \nabla_H^2 \frac{\partial \bar{\phi}}{\partial \zeta} - \frac{\partial^2 \bar{\phi}}{\partial r_0 \partial \zeta} \nabla_H^2 \left(\frac{\partial \phi}{\partial \zeta} \right) \right] dl + \int_{S_\infty} \left(\phi \frac{\partial \bar{\phi}}{\partial n} - \bar{\phi} \frac{\partial \phi}{\partial n} \right) ds = 0. \quad (70)$$

Substituting the crack conditions Eqs. (20) and (21) into the first term on the left-hand side of Eq. (70), then performing the integration with respect to θ_0 by parts, we have the result equal to zero. Substituting Eqs. (44) and (66) into the remaining terms of Eq. (70), we have

$$0 = \lim_{r_0 \rightarrow +\infty} \text{Re} \left\{ e^{-i\pi/4} \sqrt{\frac{2k_0 r_0}{\pi}} \int_{-\pi}^{+\pi} \bar{U}(\theta_0) \times [1 + \cos(\theta_0)] e^{ik_0 r_0 [1 - \cos(\theta_0)]} d\theta_0 \right\} + 4F, \quad (71)$$

for the incoming wave direction $\beta = 0$, as has been assumed. The integral in the above equation can be performed asymptotically through the method of stationary phase.³¹ This gives

$$F = -\text{Re}[U(0)], \quad (72)$$

which will be used later as a partial check of the numerical results. Here, it should be noted that Eq. (72) is in fact a result of energy conservation, or when the wave propagates to infinity, the energy must be conserved.

IV. NUMERICAL RESULTS

The typical parameters of the ice sheet are taken to be

$$\begin{aligned} E &= 5 \text{ G Pa}, \nu = 0.3, \rho_i = 922.5 \text{ kg m}^{-3}, \\ \rho_w &= 1025 \text{ kg m}^{-3}, H = 100 \text{ m}, \end{aligned} \quad (73)$$

which are the same as those in the work of Sturova.³⁶ All the results will be presented in the dimensionless form, based on the combinations of radius of the circular crack a , density of water ρ_w , and acceleration due to gravity $g = 9.80 \text{ m s}^{-2}$. To conduct numerical computations, the infinite series in Eq. (36) is truncated at a finite number, i.e., $0 \leq \ell \leq M$, while the symmetry is taken into account. The semi-infinite integrals in Eqs. (57), (58), (60), and (61) are truncated at a sufficiently large k , which can be estimated through the decay rate of the integrand.

We first consider the jump of displacement and the jump of slope across the circular crack, which can be obtained through Eq. (36) as

$$\eta^d(\theta) = \frac{1}{i\omega} [A_0 + 2 \sum_{\ell=1}^{+\infty} A_\ell \cos(\ell\theta)]$$

and

$$\eta_r^d(\theta) = \frac{1}{i\omega} [B_0 + 2 \sum_{\ell=1}^{+\infty} B_\ell \cos(\ell\theta)]. \quad (74)$$

A convergence study is carried out with respect to M . Figure 2 shows $|\eta^d|/\Lambda$ and $|\eta_r^d|/\Lambda$ against the angle θ along the crack at $k_0 = 3.0$. As the problem is symmetric about the $O-xz$ plane, results are presented only for $\theta \in [-\pi, 0]$. It can be seen from Fig. 2 that there is no visible graphic difference in the results obtained, respectively, by $M = 10$ and $M = 20$, which shows that the convergence with M has been achieved. In the following text, all the numerical results are obtained by taking $M = 10$ if it is not specifically specified. To further verify the accuracy of

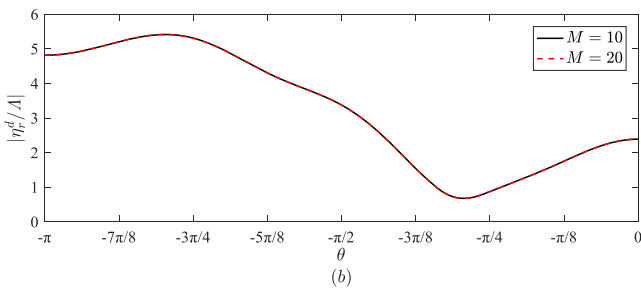
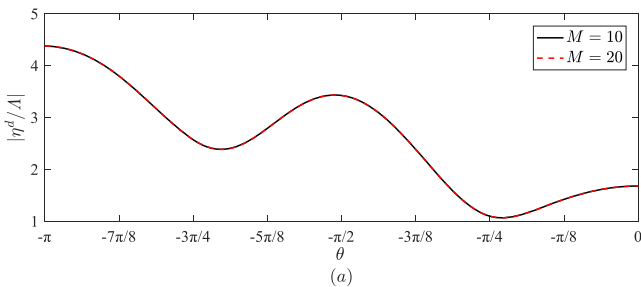


FIG. 2. Convergence study with M through the modulus of the jump of displacement $|\eta^d|/\Lambda$ and that of slope $|\eta_r^d|/\Lambda$ across the crack. Solid lines: $M = 10$; dashed lines: $M = 20$ ($a = 1, k_0 = 3.0, H = 5, h = 0.05, m = 0.045, L = 0.2849$).

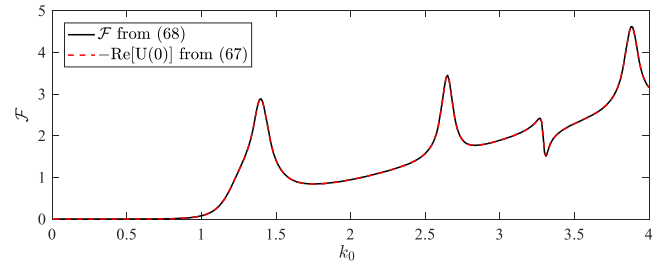


FIG. 3. Results from both sides of (72). Solid line: F from (68); dashed line: $-\text{Re}[U(0)]$ from (67) ($a = 1, H = 5, h = 0.05, m = 0.045, L = 0.2849$).

the solution procedure, in Fig. 3, we show the numerical results of both sides of Eq. (72), obtained from Eqs. (68) and (67), respectively. It can be seen from Fig. 3 that the two lines coincide with each other very well, confirming the accuracy of the solution procedure.

In Figs. 4(a) and 4(b), we show the 3D plots of η^d/Λ and $|\eta_r^d|/\Lambda$ as a function of θ and k_0 . It can be seen from Fig. 4 that when $k_0 \rightarrow 0$, we have η^d/Λ and η_r^d/Λ tend to zero for any θ , which implies that the displacement and slope are continuous across the crack. Mathematically, this is due to that when $k_0 \rightarrow 0$ or $\omega \rightarrow 0$, we have in Eq. (4) $\partial\phi/\partial z \rightarrow 0$, which means that the conditions at the circular crack in Eq. (5) hold on the whole ice sheet, and there is no difference between a continuous ice sheet and an ice sheet with a crack. Physically, when $k_0 \rightarrow 0$, the dynamic effect of the wave diminishes, i.e., the deflections of both continuous and cracked ice sheets tend to zero. As k_0 increases, the jumps of η^d/Λ and η_r^d/Λ across the crack become more pronounced. In particular, there will be more oscillations of η^d/Λ and η_r^d/Λ against θ for a larger k_0 . This is because that when k_0 increases or the wavelength $2\pi/k_0$ decreases, across the diameter of the crack, there will be much more wave cycles.

For the closed crack, an interesting point is that there may be a feature similar to resonance within the crack. From Fig. 4 which shows a 3D plot for continuous variations of η^d/Λ and η_r^d/Λ with k_0 and θ , it can be observed that there are four positions of k_0 , near which η^d/Λ and η_r^d/Λ have peaks. To show this more clearly, in Fig. 5, we provide some 2D curves for the variations of $|\eta^d|/\Lambda$ and $|\eta_r^d|/\Lambda$ against k_0 , at five different values of θ . It can be seen that the peaks occur at ranges around $k_0 = 1.41, 2.65, 3.30,$ and 3.88 , respectively, for all θ . From Eq. (74), it can be seen that the behaviors of $|\eta^d|/\Lambda$ and $|\eta_r^d|/\Lambda$ depend on those of A_ℓ and B_ℓ , which are obtained from 2×2 matrix equations of Eqs. (47) and (48). In fact, we may write Eqs. (47) and (48) as

$$[H_\ell] \{A_\ell B_\ell\}^T = \{I_B(\ell) I_S(\ell)\}^T, \quad (75)$$

where

$$[H_\ell] = \begin{bmatrix} I_B^A(\ell) & -I_B^B(\ell) \\ I_S^A(\ell) & -I_S^B(\ell) \end{bmatrix}. \quad (76)$$

It should be noticed that the term on the right-hand side of Eq. (75) is due to the incident wave, i.e., the external exciting force term. Then the natural frequency can be defined as that there are non-zero solutions of $\{A_\ell \ B_\ell\}^T$ for the zero forcing $\{I_B(\ell) \ I_S(\ell)\}^T$. This may occur when the determinant of the

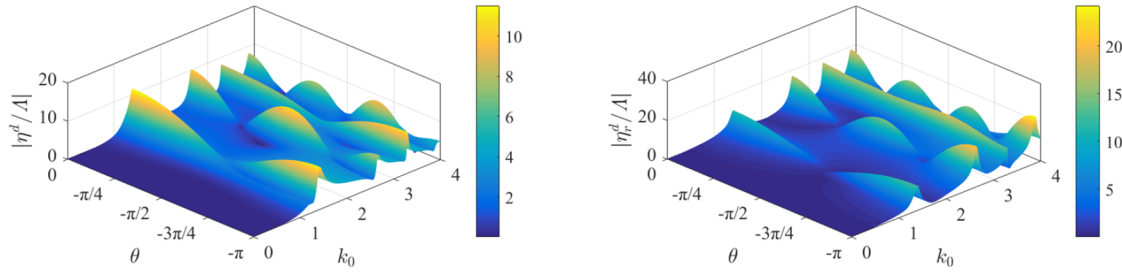


FIG. 4. Modulus of the jump of displacement η^d/Λ and that of slope η_r^d/Λ across the crack as a function of θ and k_0 ($a = 1$, $H = 5$, $h = 0.05$, $m = 0.045$, $L = 0.2849$).

matrix $[H_\ell]$ is zero, or the natural frequencies correspond to $|H_\ell| = 0$.

From a physical aspect, a solution of $|H_\ell| = 0$ will lead to a complex value for the natural frequency. In fact, if we assume an initial displacement or velocity of the ice sheet, the ice sheet will be in oscillatory motion but with a decaying amplitude due to wave energy propagation into infinity. This means that the natural frequency will be a complex value with a positive imaginary part based on the definition in Eq. (1) as a purely real value would mean that the oscillation could continue forever. As k_0 is not a complex number, when it varies, $|H_\ell|$ will not be zero. This means that A_ℓ or B_ℓ will not be infinite under the forcing term.

However, when k_0 is around an undamped natural frequency, $|H_\ell|$ is expected to be small, or A_ℓ and B_ℓ will be very large. Therefore, to explain more clearly the physics of the peaks of η^d/Λ and η_r^d/Λ , in Figs. 6(a) and 6(b), we plot the variations of $|A_\ell|$ and $|B_\ell|$ against k_0 , respectively. Here ℓ is taken from 0 to 4, beyond which A_ℓ and B_ℓ become much smaller. It can be seen within the range of k_0 in Fig. 6, each ℓ corresponds to one or more peaks. All of these peaks within $k_0 \in [0, 4]$ are reflected in Fig. 5 as all of them will contribute to the wave elevation, except for the small one at

$k_0 = 1.27$ in Fig. 6. It may be noticed that the values of η^d/Λ and η_r^d/Λ are a summation of functions containing A_ℓ and B_ℓ for $0 \leq \ell \leq M$. Thus, the positions of peaks of a specific A_ℓ and B_ℓ may not exactly correspond to those of the peaks of the final results. As it can be seen from Eq. (74), $\ell = 0, 1, 2, \dots$ correspond to the modes of deformation in the θ direction. It should be noted that for each mode ℓ , we may expect more than one peak in A_ℓ and B_ℓ , which can already be seen in Fig. 6 for $\ell = 0$ and $\ell = 1$. Generally, the magnitudes of A_ℓ and B_ℓ will decrease as ℓ increases. However, when their peaks occur, they could still be larger than magnitudes of the previous modes. All these make the ice deflection $\eta_D(r, \theta)$ highly complex.

The natural frequencies for the current problem may be related to those of a vibrating circular plate in vacuum.³⁷ When the plate is floating on the free surface, the natural frequencies are expected to be different due to the added mass effect.³⁸ Here the values of natural frequencies are expected to be different from those in the previous two cases. However, the common feature is that the resonant oscillation can occur.

The jumps of η^d/Λ and η_r^d/Λ across the crack at five different ice thicknesses h are shown in Fig. 7, with the wave

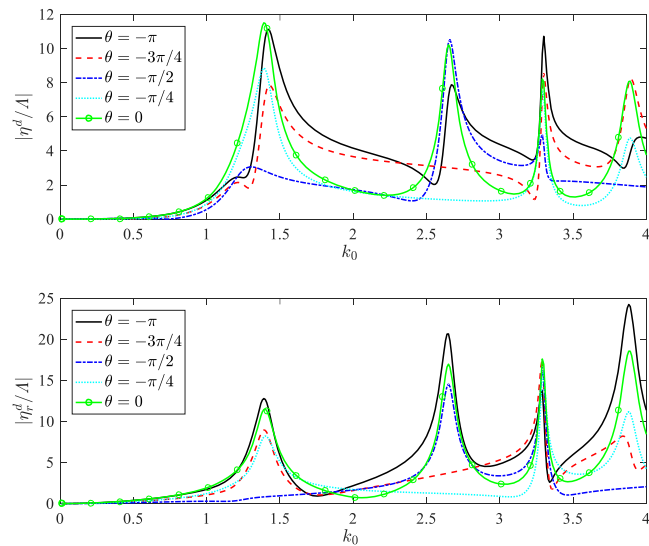


FIG. 5. Modulus of the jump of displacement η^d/Λ and that of slope η_r^d/Λ across the circular crack against k_0 at five different θ . Solid lines: $\theta = -\pi$; dashed lines: $\theta = -3\pi/4$; dash-dotted lines: $\theta = -\pi/2$; dotted lines: $\theta = -\pi/4$; solid line with open circles: $\theta = 0$ ($a = 1$, $H = 5$, $h = 0.05$, $m = 0.045$, $L = 0.2849$).

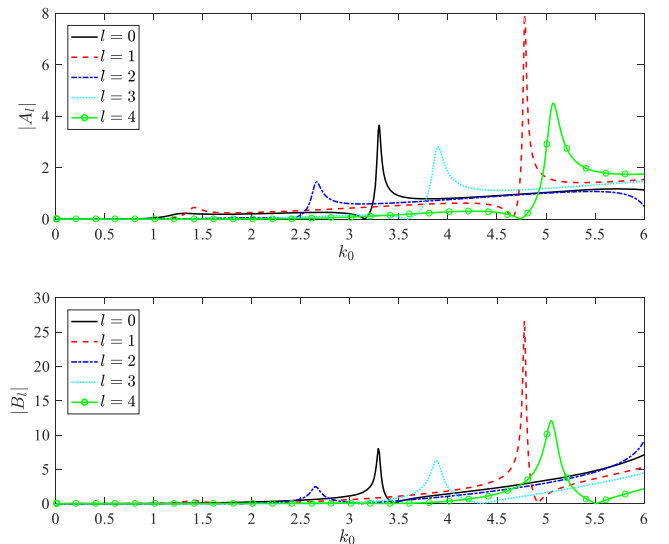


FIG. 6. Modulus of the Fourier coefficients of the jump of displacement A_ℓ and that of slope B_ℓ against k_0 for different ℓ . Solid lines: $\ell = 0$; dashed lines: $\ell = 1$; dash-dotted lines: $\ell = 2$; dotted lines: $\ell = 3$; solid line with open circles: $\ell = 4$ ($a = 1$, $H = 5$, $h = 0.05$, $m = 0.045$, $L = 0.2849$).

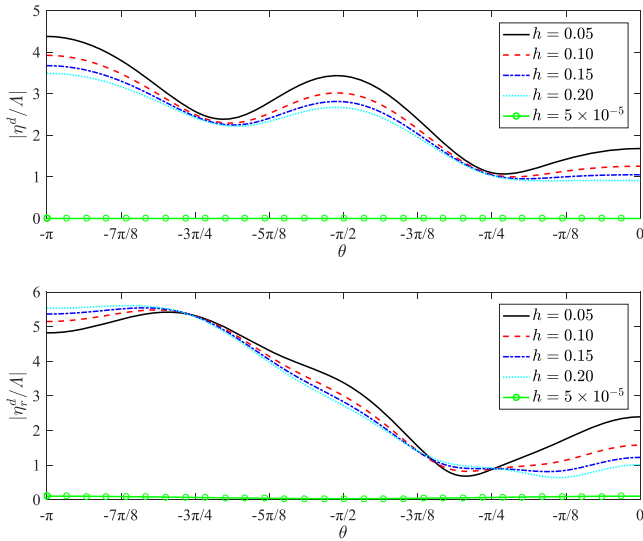


FIG. 7. Modulus of the jump of displacement η^d/Λ and that of slope η_r^d/Λ across the circular crack with different h . Solid lines: $h = 0.05$; dashed lines: $h = 0.10$; dash-dotted lines: $h = 0.15$; dotted lines: $h = 0.20$; solid line with open circles: $h = 5 \times 10^{-5}$ ($a = 1$, $k_0 = 3.0$, $H = 5$).

number taken to be $k_0 = 3.0$. At $h = 0$, there will be no ice sheet and no crack therefore exists. The wave diffraction ϕ_D should be zero, and η^d/Λ and η_r^d/Λ are also zero. To check whether the present solution procedure reflects that we let $h \rightarrow 0$, which means $L \rightarrow 0$ and $m \rightarrow 0$. Eqs. (57) and (58) become

$$I_B^A(\ell) = -a \int_0^{+\infty} k^2 J_\ell(ka) J_\ell^{(1)}(ka) dk, \quad (77)$$

$$I_B^B(\ell) = -a \int_0^{+\infty} k J_\ell(ka) J_\ell(ka) dk, \quad (78)$$

while Eqs. (60) and (61) become

$$I_S^A(\ell) = -a \int_0^{+\infty} k^3 J_\ell^{(1)}(ka) J_\ell^{(1)}(ka) dk, \quad (79)$$

$$I_S^B(\ell) = -a \int_0^{+\infty} k^2 J_\ell(ka) J_\ell^{(1)}(ka) dk. \quad (80)$$

We may note the difference between these integrals and those in Eq. (A5). Here is not a limiting process involving an exponential function in the integrand. The integrals in Eqs. (77)–(80) are divergent. Thus when $h \rightarrow 0$, the coefficients of the linear equations Eqs. (47) and (48) will tend to infinity, indicating that $A_\ell \rightarrow 0$ and $B_\ell \rightarrow 0$, which is consistent with the zero diffraction wave discussed above. Numerically, this result is reflected by the case of $h = 5 \times 10^{-5}$ in Fig. 7. As h increases, it can be seen that η^d/Λ and η_r^d/Λ become significant. The results for different h nearly follow the same oscillation pattern against θ for $0.10 \leq h \leq 0.20$ (corresponding to the dimensional thickness $1m \leq h \leq 4m$), which are within the typical range of the thickness of the polar ice sheets.³² This is not unexpected due to that the spatial variations of the ice deflection should mainly depend on the flexural gravity wavelength $2\pi/k_0$. In fact, for a fixed k_0 , considering the $1/(\omega)$ in Eq. (63), we notice that on the right-hand sides of Eqs. (47) and (48), $I_B(\ell)/\omega$ and $I_S(\ell)/\omega$ are independent of h . At the same time, as h increases, L will increase at the rate h^3 . Considering the leading terms in Eqs. (57), (58), (60), and (61),

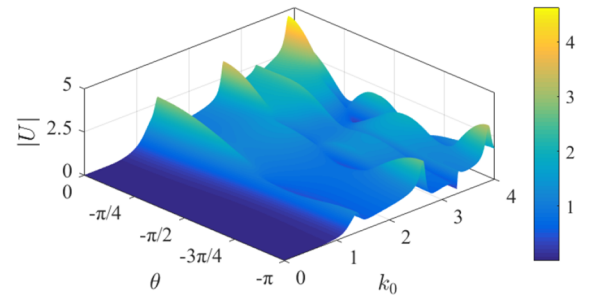


FIG. 8. Modulus of the far field diffracted wave amplitude U as a function of θ and k_0 ($a = 1$, $H = 5$, $h = 0.05$, $m = 0.045$, $L = 0.2849$).

these integrals will be not sensible to L when h is large. The same argument may be applied to Eq. (63). Thus, η_D becomes insensitive to h at a given k_0 , when h becomes relatively large. From Fig. 7, it can also be seen that the results have approximately two cycles within $\theta \in [-\pi, 0]$, which indicates that the mode corresponding to large ℓ will not have a significant effect on η_D in this case.

In Fig. 8, we show the three dimensional plot for modulus of U in Eq. (67) as a function of θ and k_0 . From Fig. 8, it can be observed that there is more diffracted wave energy propagating in the direction around $\theta = 0$, or the direction of the incoming wave. From Eqs. (67) and (63), it can be seen that both U and η_D are similar functions involving A_ℓ and B_ℓ . Therefore, similar behaviors between them can be expected. Around the natural frequencies, we can expect that U will also have large peaks, as can be observed in Fig. 8 and more clearly seen in Fig. 9. Based on Eq. (72), the result of F is shown in Fig. 10 against k_0 for different ice thicknesses h . It can be seen that for small k_0 or large wavelength, the results at different

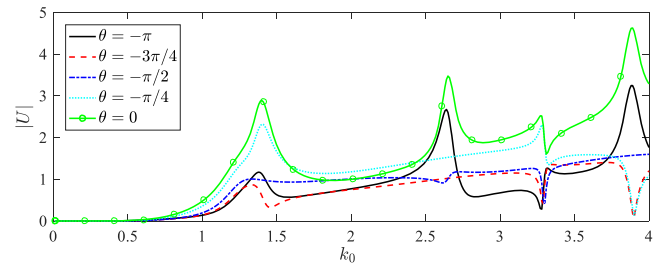


FIG. 9. Modulus of the far field diffracted wave amplitude U against k_0 at five different θ . Solid line: $\theta = -\pi$; dashed line: $\theta = -3\pi/4$; dash-dotted line: $\theta = -\pi/2$; dotted line: $\theta = -\pi/4$; solid line with open circles: $\theta = 0$ ($a = 1$, $H = 5$, $h = 0.05$, $m = 0.045$, $L = 0.2849$).

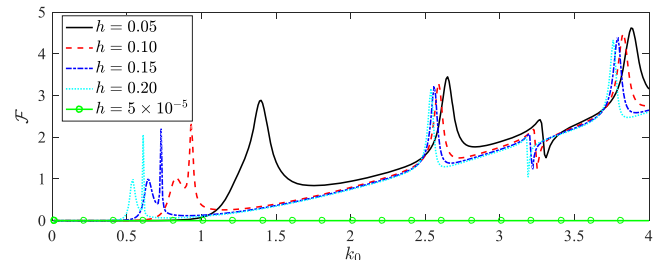


FIG. 10. The far field scattered energy F against k_0 for different h . Solid lines: $h = 0.05$; dashed lines: $h = 0.10$; dash-dotted lines: $h = 0.15$; dotted lines: $h = 0.20$; solid line with open circles: $h = 5 \times 10^{-5}$ ($a = 1$, $H = 5$).

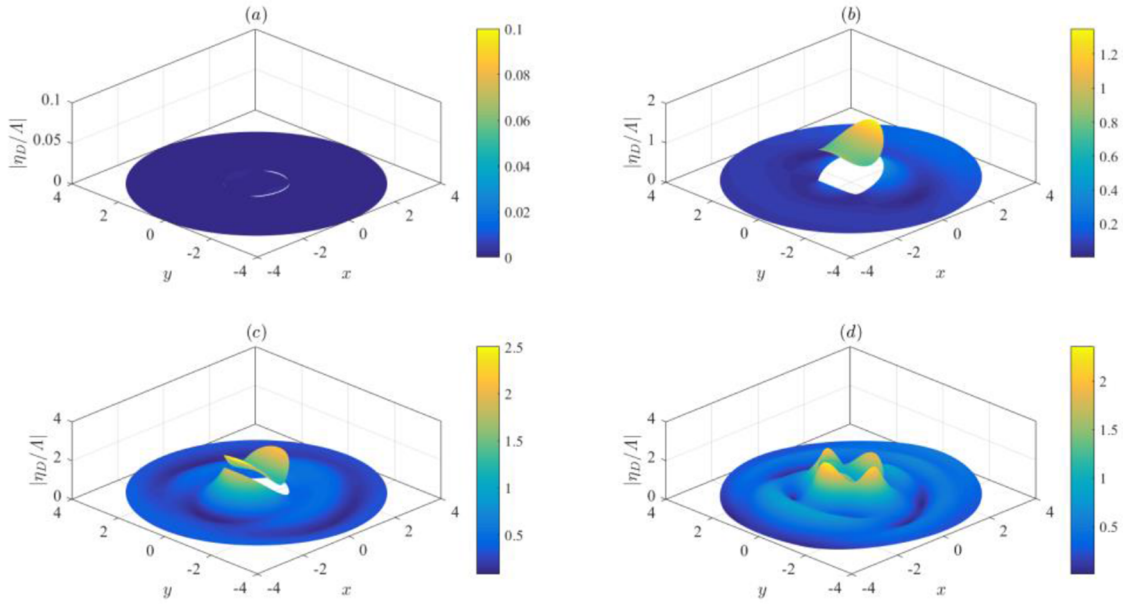


FIG. 11. Modulus of the ice deflection η_D/A at different wave numbers. (a) $k_0 = 0.1$; (b) $k_0 = 1.0$; (c) $k_0 = 2.0$; (d) $k_0 = 3.0$ ($a = 1$, $H = 5$, $h = 0.05$, $m = 0.045$, $L = 0.2849$).

h are quite different, apart from the case of $k_0 \rightarrow 0$ in which the dynamic process diminishes. This is because relatively to the wavelength, all the h in Fig. 10 is small and the effect of its variation is important. As k_0 increases or the wavelength decreases, the effect of h is less significant for the reasons discussed in Fig. 7.

Finally, results are provided for the deflection of the ice sheet. The modulus of the ice deflection $|\eta_D/A|$ due to the diffracted velocity potential ϕ_D is shown in Fig. 11 at four different wave numbers $k_0 = 0.1, 1.0, 2.0$, and 3.0 . It can be observed that when k_0 is small or the wavelength is much larger than the radius of the crack, the overall ice deflections induced by the diffracted velocity potential are quite small. When k_0 increases, it can be seen that the spatial variation of $|\eta_D/A|$ becomes fast, and the number of peaks and troughs increases. Particularly, from Fig. 11 we can observe that the large ice deflection usually happens along each side of the crack, which can be much larger than the incident wave amplitude. To further demonstrate this, computations are then carried out for the ice deflections due to the diffracted wave at six different positions near the crack against k_0 , i.e., $r = 0.999, 1.001$ for $\theta = -\pi, -\pi/2, 0$, respectively. The results are plotted in Fig. 12, together with the jumps of the ice deflection across the crack. Invoking Eq. (63), we have that $|\eta_D/A|$ is a function of A_ℓ and B_ℓ , while invoking Eq. (74), we have $|\eta^d/A|$ is a function of A_ℓ . Near the natural frequencies, both A_ℓ and B_ℓ will have large peaks, as shown in Fig. 6. Therefore, we can expect that around these frequencies, both the ice deflection near the crack and the jump of the displacement across the crack will have large peaks, as reflected in Fig. 12. However, in Fig. 12(b) for $\theta = -\pi/2$, the peaks corresponding to $k_0 = 1.41$ and 3.88 ($\ell = 1$ and 3) disappear. This is due to that the function $\cos(-\pi\ell/2)$ is zero for an odd ℓ , which means that there is no peak of $|\eta_D/A|$ and $|\eta^d/A|$ along the y -axis at the natural frequencies corresponding to an odd ℓ . Also, for the ice deflection at origin, due to $J_\ell(0) = 1$ for $\ell = 0$ and

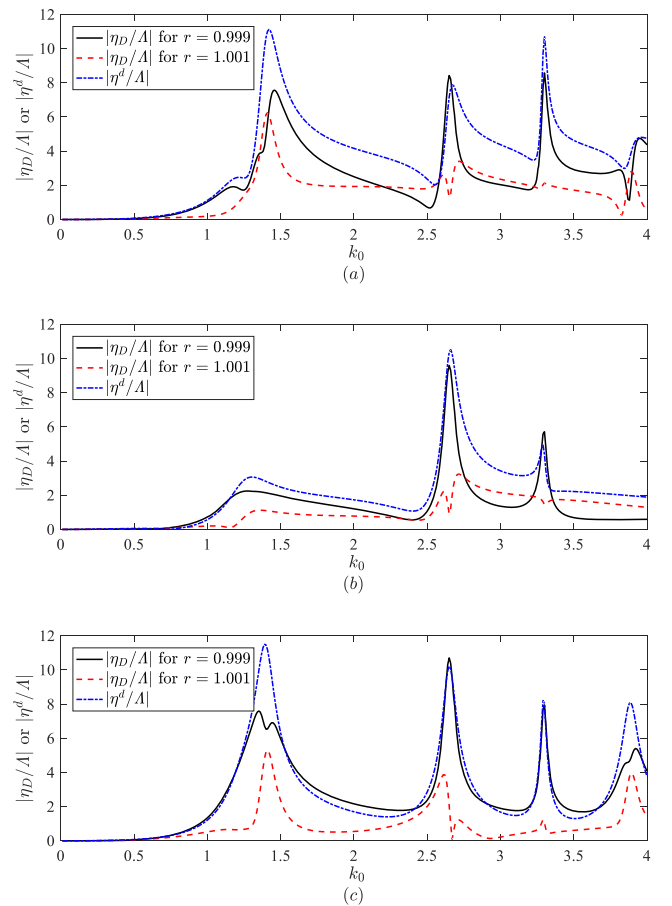


FIG. 12. Deflection of the ice sheet near the crack and its jump across the crack against k_0 at different positions. Solid lines: $|\eta_D/A|$ for $r = 0.999$; dashed lines: $|\eta_D/A|$ for $r = 1.001$; dash-dotted lines: $|\eta^d/A|$. (a) $\theta = -\pi$; (b) $\theta = -\pi/2$; (c) $\theta = 0$ ($a = 1$, $H = 5$, $h = 0.05$, $m = 0.045$, $L = 0.2849$).

$J_\ell(0) = 0$ for $\ell \neq 0$, we have $|\eta_D/A|$ will have large peaks at the natural frequencies corresponding to $\ell = 0$ only. In Fig. 13, we show the results for the ice deflection near the crack against

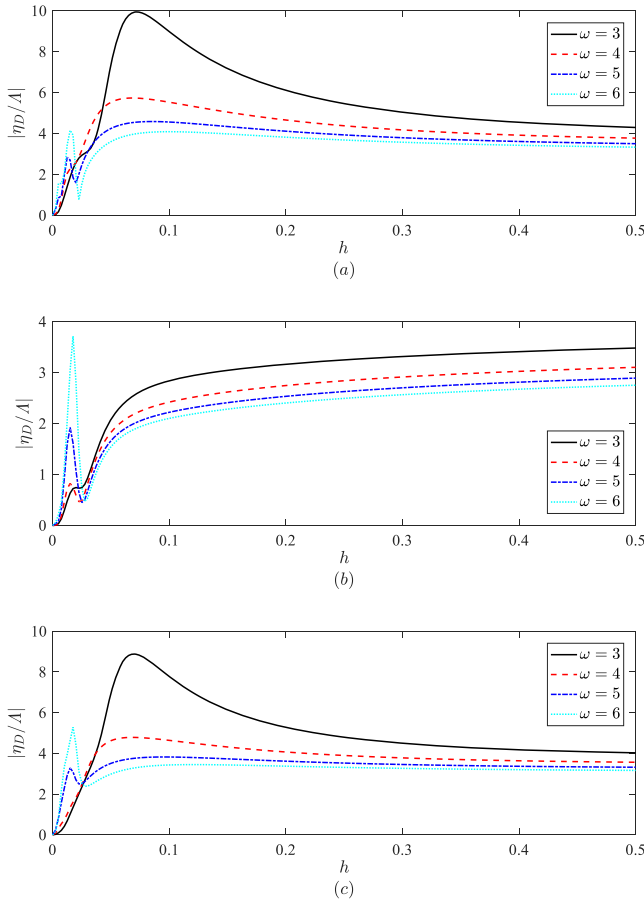


FIG. 13. Deflection of the ice sheet near the crack against h at different wave frequencies ω . Solid lines: $\omega = 3$; dashed lines: $\omega = 4$; dash-dotted lines: $\omega = 5$; dotted lines: $\omega = 6$. (a) $\theta = -\pi$; (b) $\theta = -\pi/2$; (c) $\theta = 0$ ($a = 1$, $r = 0.999$, $H = 5$).

the ice thickness h at four different wave frequencies ω . From Fig. 13, it can be seen that the ice deflection $|\eta_D|/A$ increases with h rapidly when h is small, and when h becomes further larger, the variation of $|\eta_D|/A$ is not obvious. We may notice that in contrast to Fig. 7, for a fixed ω , k_0 will change with h . It is possible that k_0 can be at a value leading to a minimal $|H_\ell|$ in Eq. (75) and therefore a resonant behavior. This can be seen in Fig. 13 at $h = 0.0175$, 0.0150 , 0.0150 , and 0.0175 corresponding to $k_0 = 2.3063$, 2.8053 , 3.0755 , and 3.0485 , respectively, for $\omega = 3, 4, 5$, and 6 .

V. CONCLUSIONS

In this paper, we have presented the solution for the wave diffraction by a circular crack in an ice sheet floating on water of finite depth, based on the linear velocity potential theory for the fluid flow and thin elastic plate theory for the ice sheet. The procedure starts from the integral equation involving the Green function for an ice sheet without the crack. For the circular crack, the unknown jumps of the displacement and slope of the ice sheet at the crack are expanded into a Fourier series and a semi-analytical solution is obtained. For a crack of an arbitrary shape, the principle of the integral equation in this paper can still be used. The crack can be discretized into small segments, and solution can be obtained

numerically, as commonly performed in the boundary element method.

The convergence study has been carried out with respect to the number of terms kept in the Fourier series, through the jumps of displacement and slope across the crack. The result shows that the series converges very fast. The obtained jumps show oscillatory behaviors with the wave number, which is found to be related to the natural modes of the ice sheet or the resonance can occur when the incoming wave frequency corresponds to one of the natural frequencies of the ice sheet. This is analyzed through the behavior of the coefficients of the Fourier series. Similar resonant behaviors of the far field wave amplitude, the total scattered wave energy, and the ice deflections are also observed. Also, near the natural frequencies, the ice deflections on both sides of the crack and their jumps across the crack will all have large peaks.

For the effect of the ice thickness h , the solution procedure will give a zero diffracted velocity potential when the upper surface tends to a free surface, and this is consistent with the physics. At small wave number k_0 , the variation of h has a significant effect on the ice sheet deflection, due to the fact that h is small compared to the wavelength. When the fixed k_0 is relatively larger, as h increases, its effects become less significant. For a given wave frequency ω , when h is small, the ice sheet deflection increases with h rapidly. The natural frequencies of the ice sheet vary with h continuously. When ω is near one of the natural frequencies, large peaks of the results are observed.

The solution procedure can be also used to solve the infinite water depth problem, as given in Appendix B. Together with the numerical method mentioned above, other cases including pressure load on the ice sheet and the effect of ocean current can also be considered.

ACKNOWLEDGMENTS

This work was supported by Lloyd's Register Foundation through the joint centre involving University College London, Shanghai Jiaotong University, and Harbin Engineering University, to which the authors are most grateful. Lloyd's Register Foundation helps to protect life and property by supporting engineering-related education, public engagement, and the application of research. This work is also supported by the National Natural Science Foundation of China (Grant Nos. 51879123 and 51709131).

APPENDIX A: TREATMENT OF THE IMPROPER INTEGRALS

In each of the integrands of Eqs. (49)–(54), the leading order of k in the numerator is higher than that in the corresponding denominator. This can be problematic when $\zeta \rightarrow 0^-$ as the integral becomes divergent if the limit is taken before the integration. To resolve this, we may adopt the method similar to that used in the 2D problem.²⁹ We have³⁹

$$\frac{P_u^0(\cos \vartheta)}{r_1^{u+1}} = \frac{1}{u!} \int_0^{+\infty} e^{k\zeta} k^u J_0(kR) dk, \quad (\text{A1})$$

where P_u^0 is the Legendre function,³⁵ with $R = r_1 \sin \vartheta$ and $\zeta = -r_1 \cos \vartheta$. Substituting Eq. (38) into Eq. (A1), we obtain

$$\frac{P_u^0(\cos \vartheta)}{r_1^{u+1}} = \frac{1}{u!} \sum_{\ell=-\infty}^{+\infty} e^{-i\ell(\theta-\theta_0)} \int_0^{+\infty} e^{k\zeta} k^u J_\ell(kr_0) J_\ell(kr) dk. \quad (\text{A2})$$

When $\zeta \rightarrow 0^-$ or $\cos \vartheta \rightarrow 0$, we have³⁵

$$P_u^0(0) = \cos(u\pi/2) \Gamma(u/2 + 1/2) / [\sqrt{\pi} \Gamma(u/2 + 1)], \quad (\text{A3})$$

where $\Gamma(u)$ is the Gamma function.³⁵ When u is an odd number, $P_u^0(0)$ in Eq. (A3) is zero. Since the right-hand side of Eq. (A2) is a Fourier series of $(\theta - \theta_0)$, its coefficient or each of the integrals is zero for an odd u as $\zeta \rightarrow 0^-$, or

$$\lim_{\zeta \rightarrow 0^-} \int_0^{+\infty} e^{k\zeta} k^u J_\ell(kr_0) J_\ell(kr) dk = 0 \quad \text{for an odd } u > 0. \quad (\text{A4})$$

We may take s_1 -th and s_2 -th order derivatives with respect to r_0 and r in Eq. (A4), respectively. This gives

$$I(\tilde{u}, s_1, s_2) = \lim_{\zeta \rightarrow 0^-} \int_0^{+\infty} e^{k\zeta} k^{\tilde{u}} J_\ell^{(s_1)}(kr_0) J_\ell^{(s_2)}(ka) dk = 0, \quad (\text{A5})$$

provided $u = \tilde{u} - s_1 - s_2 > 0$ is an odd number.

In Eqs. (49) and (50), (52), and (53), we also have the cases with $u \leq 0$ in Eq. (A5), in particular $I(0, s_1, s_2)$ and $I(1, 1, 1)$. For the first one, it can be explicitly obtained directly. We have when $r_0 = a$

$$I(0, 0, 1) = I(0, 1, 0) = 0, \quad \ell > 0 = -\frac{1}{2a}, \quad \ell = 0. \quad (\text{A6})$$

For $I(1, 1, 1)$, we may use³⁵

$$J_\ell^{(1)}(kr) = \frac{J_{\ell-1}(kr) - J_{\ell+1}(kr)}{2}, \quad (\text{A7})$$

and

$$J_\ell^{(1)}(kr_0) = J_{\ell-1}(kr_0) - \frac{\ell}{kr_0} J_\ell(kr_0), \quad (\text{A8})$$

$$J_\ell^{(1)}(kr_0) = -J_{\ell+1}(kr_0) + \frac{\ell}{kr_0} J_\ell(kr_0). \quad (\text{A9})$$

By first replacing $J_\ell^{(1)}(ka)$ with Eq. (A7), then using Eq. (A8) for the term related to $J_{\ell-1}^{(1)}(ka)$ and Eq. (A9) for the term related to $J_{\ell+1}^{(1)}(ka)$, we can write

$$\begin{aligned} I(1, 1, 1) &= \frac{1}{2} \lim_{\zeta \rightarrow 0^-} \int_0^{+\infty} e^{k\zeta} k J_{\ell-1}(kr_0) J_{\ell-1}(ka) dk \\ &+ \frac{1}{2} \lim_{\zeta \rightarrow 0^-} \int_0^{+\infty} e^{k\zeta} k J_{\ell+1}(kr_0) J_{\ell+1}(ka) dk \\ &- \frac{1}{2} \frac{\ell}{r_0} \lim_{\zeta \rightarrow 0^-} \int_0^{+\infty} e^{k\zeta} J_\ell(kr_0) J_{\ell-1}(ka) dk \\ &- \frac{1}{2} \frac{\ell}{r_0} \lim_{\zeta \rightarrow 0^-} \int_0^{+\infty} e^{k\zeta} J_\ell(kr_0) J_{\ell+1}(ka) dk, \quad (\text{A10}) \end{aligned}$$

or

$$\begin{aligned} I(1, 1, 1) &= -\frac{1}{2} \frac{\ell}{r_0} \left[\int_0^{+\infty} J_\ell(kr_0) J_{\ell-1}(ka) dk \right. \\ &\left. + \int_0^{+\infty} J_\ell(kr_0) J_{\ell+1}(ka) dk \right], \quad (\text{A11}) \end{aligned}$$

in which Eq. (A4) have been used. By further using³⁵

$$\begin{aligned} \int_0^{+\infty} J_\ell(kr_0) J_{\ell-1}(kr) dk &= \frac{r^{\ell-1}}{r_0^\ell}, \quad 0 < r < r_0 \\ &= \frac{1}{2r}, \quad 0 < r = r_0 = 0, \quad r > r_0 > 0 \quad \text{for } \ell > 0, \quad (\text{A12}) \end{aligned}$$

we have when $r_0 = a$

$$I(1, 1, 1) = -\frac{\ell}{2a^2} \quad \text{for } \ell \geq 0. \quad (\text{A13})$$

With the above results, we consider the integral of the following form:

$$\tilde{I} = \lim_{\substack{\zeta \rightarrow 0^- \\ r_0 \rightarrow a}} \int_L \frac{k Z^{(1)}(\zeta)}{K(\omega, k) Z(0)} k^{\tilde{u}+3} J_\ell^{(s_1)}(kr_0) J_\ell^{(s_2)}(ka) dk, \quad (\text{A14})$$

in which the order of k in the numerator may be higher than that in the denominator. Invoking Eq. (10), we can write \tilde{I} as

$$\begin{aligned} \tilde{I} &= \frac{1}{L} \left\{ \int_L \frac{\rho_w \omega^2 - (\rho_w g - m \omega^2) k \tanh(kH)}{K(\omega, k)} \right. \\ &\left. \times k^{\tilde{u}} J_\ell^{(s_1)}(ka) J_\ell^{(s_2)}(ka) dk + \tilde{I}_1 \right\}, \quad (\text{A15}) \end{aligned}$$

where

$$\tilde{I}_1 = \lim_{\substack{\zeta \rightarrow 0^- \\ r_0 \rightarrow a}} \int_L \frac{Z^{(1)}(\zeta)}{Z^{(1)}(0)} k^{\tilde{u}} J_\ell^{(s_1)}(kr_0) J_\ell^{(s_2)}(ka) dk. \quad (\text{A16})$$

We may rewrite Eq. (A16) as

$$\begin{aligned} \tilde{I}_1 &= \lim_{\substack{\zeta \rightarrow 0^- \\ r_0 \rightarrow a}} \int_L \left[\frac{Z^{(1)}(\zeta)}{Z^{(1)}(0)} - e^{k\zeta} \right] k^{\tilde{u}} J_\ell^{(s_1)}(kr_0) J_\ell^{(s_2)}(ka) dk \\ &+ \lim_{r_0 \rightarrow a} \mathcal{I}(\tilde{u}, s_1, s_2). \quad (\text{A17}) \end{aligned}$$

When the limit $\zeta \rightarrow 0^-$ is taken, the first term on the right-hand side of Eq. (A17) is zero, or

$$\tilde{I}_1 = \lim_{r_0 \rightarrow a} \mathcal{I}(\tilde{u}, s_1, s_2). \quad (\text{A18})$$

APPENDIX B: SOLUTION FOR INFINITE WATER DEPTH

The case of infinite water depth is merely a special case of the present work. When $H \rightarrow +\infty$, the Green function G in Eq. (18) becomes

$$G = \frac{1}{r_1} + \frac{1}{r_3} + 2\rho_w \omega^2 \int_L \frac{e^{+k(z+\zeta)}}{K(\omega, k)} J_0(kR) dk, \quad (\text{B1})$$

where r_3 is the distance between the field point p and the mirror image of the sink point q about the mean upper surface $z = 0$, and the dispersion equation $K(\omega, k)$ in Eq. (10) becomes

$$K(\omega, k) \equiv (Lk^4 + \rho_w g - m \omega^2) k - \rho_w \omega^2. \quad (\text{B2})$$

For the diffracted velocity potential, ϕ_D in Eq. (40) can be written as

$$\begin{aligned} \phi_D &= \frac{L}{a^2} \sum_{\ell=-\infty}^{+\infty} e^{i\ell\theta_0} \int_L \frac{ke^{+k\zeta}}{K(\omega, k)} J_\ell(kr_0) \\ &\times [A_\ell F_1(k, \ell) - B_\ell F_2(k, \ell)] dk, \quad (\text{B3}) \end{aligned}$$

while for the incident potential ϕ_I , $\psi(\zeta)$ in Eq. (45) becomes

$$\psi(\zeta) = e^{+k_0\zeta}. \quad (\text{B4})$$

The linear equations (47) and (48) for A_ℓ and B_ℓ maintain the same forms, while Eq. (59) can be simplified as

$$K_1 = k^2 \text{ and } K_2 = \rho_w \omega^2 - (\rho_w g - m\omega^2)k. \quad (\text{B5})$$

The ice deflection η_D in Eq. (63) becomes

$$\eta_D = \frac{1}{i\omega} \frac{L}{a^2} \sum_{\ell=-\infty}^{+\infty} e^{i\ell\theta_0} \int_L \frac{k^2 J_\ell(kr_0)}{K(\omega, k)} \times [A_\ell F_1(k, \ell) - B_\ell F_2(k, \ell)] dk. \quad (\text{B6})$$

For the diffracted velocity potential ϕ_D in the far field, Eq. (66) becomes

$$\lim_{r_0 \rightarrow +\infty} \phi_D = \sqrt{\frac{2}{\pi k_0 r_0}} e^{+k_0\zeta} e^{-i(k_0 r_0 - \pi/4)} IU(\theta_0), \quad (\text{B7})$$

where

$$U(\theta_0) = -i\pi \frac{k_0}{I} \frac{1}{K'(\omega, k_0)} \frac{L}{a^2} \sum_{\ell=-\infty}^{+\infty} e^{i\ell(\theta_0 + \pi/2)} \times [A_\ell F_1(k_0, \ell) - B_\ell F_2(k_0, \ell)]. \quad (\text{B8})$$

- ¹C. O. Collins, W. E. Rogers, A. Marchenko, and A. V. Babanin, "In situ measurements of an energetic wave event in the Arctic marginal ice zone," *Geophys. Res. Lett.* **42**, 1863, <https://doi.org/10.1002/2015gl063063> (2015).
- ²V. A. Squire, "Past, present and impending hydroelastic challenges in the polar and subpolar seas," *Philos. Trans. R. Soc., A* **369**, 2813 (2011).
- ³G. Q. Robin, "Wave propagation through fields of pack ice," *Philos. Trans. R. Soc., A* **255**, 313 (1963).
- ⁴A. L. Kohout, M. J. Williams, S. M. Dean, and M. H. Meylan, "Storm-induced sea-ice breakup and the implications for ice extent," *Nature* **509**, 604 (2014).
- ⁵V. A. Squire, W. H. Robinson, P. J. Langhorne, and T. G. Haskell, "Vehicles and aircraft on floating ice," *Nature* **333**, 159 (1988).
- ⁶C. Fox and V. A. Squire, "On the oblique reflexion and transmission of ocean waves at shore fast sea ice," *Philos. Trans. R. Soc., A* **347**, 185 (1994).
- ⁷N. J. Balmforth and R. V. Craster, "Ocean waves and ice sheets," *J. Fluid Mech.* **395**, 89 (1999).
- ⁸C. M. Linton and H. Chung, "Reflection and transmission at the ocean/sea-ice boundary," *Wave Motion* **38**, 43 (2003).
- ⁹P. Brocklehurst, A. A. Korobkin, and E. I. Pärä, "Interaction of hydroelastic waves with a vertical wall," *J. Eng. Math.* **68**, 215 (2010).
- ¹⁰A. A. Korobkin, T. I. Khabakhpasheva, and A. A. Papin, "Waves propagating along a channel with ice cover," *Eur. J. Mech.: B/Fluids* **47**, 166 (2014).
- ¹¹M. H. Meylan and V. A. Squire, "Response of a circular ice floe to ocean waves," *J. Geophys. Res.: Oceans* **101**, 8869, <https://doi.org/10.1029/95jc03706> (1996).
- ¹²M. A. Pete, M. H. Meylan, and H. A. Chung, "Wave scattering by a circular elastic plate in water of finite depth: A closed form solution," *Int. J. Offshore Polar Eng.* **14**, 81 (2004).
- ¹³F. Montiel, F. Bonnefoy, P. Ferrant, L. G. Bennetts, V. A. Squire, and P. Marsault, "Hydroelastic response of floating elastic discs to regular waves. Part 1. Wave basin experiments," *J. Fluid Mech.* **723**, 604 (2013).
- ¹⁴F. Montiel, L. G. Bennetts, V. A. Squire, F. Bonnefoy, and P. Ferrant, "Hydroelastic response of floating elastic discs to regular waves. Part 2. Modal analysis," *J. Fluid Mech.* **723**, 629 (2013).
- ¹⁵F. Montiel, V. A. Squire, and L. G. Bennetts, "Attenuation and directional spreading of ocean wave spectra in the marginal ice zone," *J. Fluid Mech.* **790**, 492 (2016).
- ¹⁶F. Montiel and V. A. Squire, "Modelling wave-induced sea ice break-up in the marginal ice zone," *Proc. R. Soc. A* **473**, 20170258 (2017).
- ¹⁷C. D. Wang and M. H. Meylan, "A higher-order-coupled boundary element and finite element method for the wave forcing of a floating elastic plate," *J. Fluids Struct.* **19**, 557 (2004).
- ¹⁸T. D. Williams and V. A. Squire, "Scattering of flexural-gravity waves at the boundaries between three floating sheets with applications," *J. Fluid Mech.* **569**, 113 (2006).
- ¹⁹D. Porter and R. Porter, "Approximations to wave scattering by an ice sheet of variable thickness over undulating bed topography," *J. Fluid Mech.* **509**, 145 (2004).
- ²⁰L. G. Bennetts, N. R. T. Biggs, and D. Porter, "A multi-mode approximation to wave scattering by ice sheets of varying thickness," *J. Fluid Mech.* **579**, 413 (2007).
- ²¹L. G. Bennetts and T. D. Williams, "Wave scattering by ice floes and polynyas of arbitrary shape," *J. Fluid Mech.* **662**, 5 (2010).
- ²²M. D. Barrett and V. A. Squire, "Ice-coupled wave propagation across an abrupt change in ice rigidity, density, or thickness," *J. Geophys. Res.: Oceans* **101**, 20825, <https://doi.org/10.1029/96jc01920> (1996).
- ²³V. A. Squire and T. W. Dixon, "An analytic model for wave propagation across a crack in an ice sheet," *Int. J. Offshore Polar Eng.* **10**, 173 (2000).
- ²⁴T. D. Williams and V. A. Squire, "Wave propagation across an oblique crack in an ice sheet," *Int. J. Offshore Polar Eng.* **12**, 157 (2002).
- ²⁵D. V. Evans and R. Porter, "Wave scattering by narrow cracks in ice sheets floating on water of finite depth," *J. Fluid Mech.* **484**, 143 (2003).
- ²⁶R. Porter and D. V. Evans, "Flexural-gravity wave diffraction by finite cracks of arbitrary shape in ice sheets," in *The 19th International Workshop on Water Waves and Floating Bodies*, Cortona, Italy, 2004.
- ²⁷R. Porter and D. V. Evans, "Scattering of flexural waves by multiple narrow cracks in ice sheets floating on water," *Wave Motion* **43**, 425 (2006).
- ²⁸R. Porter and D. V. Evans, "Diffraction of flexural waves by finite straight cracks in an elastic sheet over water," *J. Fluids Struct.* **23**, 309 (2007).
- ²⁹Z. F. Li, G. X. Wu, and C. Y. Ji, "Wave radiation and diffraction by a circular cylinder submerged below an ice sheet with a crack," *J. Fluid Mech.* **845**, 682 (2018).
- ³⁰Z. F. Li, G. X. Wu, and C. Y. Ji, "Interaction of wave with a body submerged below an ice sheet with multiple arbitrarily spaced cracks," *Phys. Fluids* **30**, 057107 (2018).
- ³¹C. C. Mei, M. Stiassnie, and K. P. Yue, *Theory and Applications of Ocean Surface Waves Part 1: Linear Aspects* (World Scientific Publishing, Singapore, 2005).
- ³²V. A. Squire, J. P. Dugan, P. Wadhams, P. J. Rottier, and A. K. Liu, "Of ocean waves and sea ice," *Annu. Rev. Fluid Mech.* **27**, 115 (1995).
- ³³V. A. Squire, "Of ocean waves and sea-ice revisited," *Cold Reg. Sci. Technol.* **49**, 110 (2007).
- ³⁴J. V. Wehausen and E. V. Laitone, *Surface Waves* (Springer Verlag, Berlin, 1960).
- ³⁵M. Abramowitz and I. A. Stegun, *Handbook of Mathematical Functions* (Dover Press, New York, 1965).
- ³⁶I. V. Sturova, "Radiation of waves by a cylinder submerged in water with ice floe or polynya," *J. Fluid Mech.* **784**, 373 (2015).
- ³⁷K. Itao and S. H. Crandall, "Natural modes and natural frequencies of uniform, circular, free-edge plates," *J. Appl. Mech.* **46**, 448 (1979).
- ³⁸M. K. Kwak, "Vibration of circular plates in contact with water," *J. Appl. Mech.* **58**, 480 (1991).
- ³⁹F. Ursell, "On the wave motion near a submerged sphere between parallel walls: I. Multipole potentials," *Q. J. Mech. Appl. Math.* **52**, 585 (1999).